J Mater Sci: Mater Med (2011) 22:1947–1964
DOI 10.1007/s10856-011-4370-z

Chitosan/silk fibroin-based tissue-engineered graft seeded with adipose-derived stem cells enhances nerve regeneration in a rat model

Yujun Wei · Kai Gong · Zhenghuan Zheng · Aijun Wang · Qiang Ao · Yandao Gong · Xiufang Zhang

Received: 13 January 2011 / Accepted: 30 May 2011 / Published online: 8 June 2011

Abstract Sciatic nerve injury presents an ongoing challenge in reconstructive surgery. Local stem cell application has recently been suggested as a possible novel therapy. In the present study we evaluated the potential of a chitosan/silk fibroin scaffold serving as a delivery vehicle for adipose-derived stem cells and as a structural framework for the injured nerve regeneration. The cell-loaded scaffolds were used to regenerate rat sciatic nerve across a 10 mm surgically-induced sciatic nerve injury. The functional nerve recovery was assessed by both walking track and histology analysis. Results showed that the reconstruction of the injured sciatic nerve had been significantly enhanced with restoration of nerve continuity and function recovery in the cell-loaded scaffold groups, and their target skeletal muscle had been extensively reinnervated. This study raises a potential possibility of using the newly developed nerve grafts as a promising alternative for nerve regeneration.

1 Introduction

Peripheral nerve regeneration of partial injuries, such as nerve crushes, entrapment with nerve compression, and trauma-induced or iatrogenic neurotmesis with incomplete nerve transaction, occurs frequently [1]. Functional recovery following surgical nerve repair is often disappointing and remains a challenge despite continued improvements in microsurgical techniques and tissue engineering.

Incomplete recovery is due to several factors including scar formation at the lesion site. Following nerve injury and repair, fibroblasts invade the lesion site and establish a physical obstruction. Extraneural scarring may lead to nerve tethering to adjacent tissues, which prevents nerve mobility and induces traction injuries and vasospasm. Physical obstructions may reduce axonal re-growth through lesion sites and consequently impair function [2]. Various procedures have been developed to prevent extraneural scarring, including wrapping nerves with veins, muscle, fat, fascia, free vascularized omentum and polymeric membranes seeded with Schwann cells or olfactory ensheathing cells [3–5]. However, the results are often inconsistent.

For theses reasons, recent studies have focused on improving bioengineered scaffolds by mimicking features of the permissive environment in the peripheral nervous system following injury [6–8]. Our aim was to develop a therapeutic chitosan (CS)/silk fibroin (SF) scaffold by seeding with regenerative cells. The scaffold would act as a baffle to physically block fibroblast invasion into the lesion area, reduce scar tissue and be a three-dimensional carrier for cell transplantation. Bioartificial scaffolds for cell transplantation is an alternative strategy to create a favorable environment for nerve regeneration. In our study, we compare scaffolds alone or seeded with regenerative cells including primary Schwann cells (SCs) and adipose-derived stem cells (ADSCs) for nerve regeneration.

CS, a naturally degradable polysaccharide composed of alternating acetylated and deacetylated D-glucosamine residues, has been clinically applied in hemostatic wound

Y. Wei · K. Gong · Z. Zheng · Y. Gong · X. Zhang (✉)
School of Life Sciences, State Key Laboratory of Biomembrane and Membrane Biotechnology, Tsinghua University, Beijing 100084, China
e-mail: zxf-dbs@mail.tsinghua.edu.cn

A. Wang
Department of Bioengineering, University of California, Berkeley, CA 94720, USA

Q. Ao
Department of Neurosurgery of Yuquan Hospital, Tsinghua University, Beijing 100049, China

dressings and is a promising component of novel biocompatible matrices in tissue engineering [9]. CS shares similar properties with polysaccharide and glycosaminoglycan components of the extracellular matrix (ECM), which allow CS to function as a substrate for cell adhesion, migration, and ultimately tissue incorporation [10]. In our previous study, we demonstrated high in vitro CS biocompatibility with nerve cells [11]. However, the use of CS for tissue-engineering nerve grafts remains uncharacterized. Recent advances in CS optimization in terms of biocompatibility and cell support have been achieved by hybridization with the structural SF protein [9].

SF is a natural fibrous protein, which is useful for surgical implantation due to advantageous biological characteristics. These characteristics include oxygen and water permeability, cell attachment and proliferation support, relatively low thrombogenicity, a low inflammatory response and protease susceptibility, and most importantly, high degradation kinetics and solid physical strength with flexibility [12]. Previous studies demonstrated that SF fibers are biocompatible with peripheral nerve tissues and cells [13]. Other studies have shown that the combination of SF with CS improves SF structural features, which benefit from CS surface chemistry and produce a hybrid scaffold with ideal qualities for cell attachment and population of the scaffold [9, 12].

SC transplantation is a promising therapy following peripheral nerve transection. SCs and basal lamina provide two key factors for nerve regeneration: (1) acting as a scaffold for regenerating axons that grow through empty basal lamina tubes [14]; (2) secretion of numerous neurotrophic factors that improve nerve regeneration [15, 16]. However, their clinical use is limited by culturing an adequate quantity of SCs for transplantation into nerve conduits, which is time consuming and technically challenging. Moreover, SCs are not easily accessible and require an autologous nerve biopsy with the related complications of anesthesia and pain at the harvest site [14, 17]. However, with the increasing clinical use of stem cells, new strategies are being developed for the treatment of nerve injuries [18].

Recently, ADSCs have been identified as a source of adult stem cells. ADSCs can differentiate into various cell types from mesodermal to ectodermal lineages such as adipocytes [19], osteoblasts [20], myocytes [21], chondrocytes [22], endothelial cells [23], cardiomyocytes [24] and neural lineages [25–27]. In a previous study, we demonstrated that ADSCs can be induced to differentiate into Schwann-like cells by an indirect co-culture microenvironment [28]. Furthermore, ADSCs proliferate rapidly in culture and are easily isolated by conventional liposuction procedures that avoid tissue morbidity compared with that of bone marrow aspiration. Similar to other stem cell types, the potential of ADSCs for regeneration was initially considered to be related to their differentiation potential. Although this assumption is true, there is an increasing body of evidence describing trophic effects of ADSCs on protection, survival and differentiation of various in vivo cells/tissues [29]. Moreover, ADSCs have demonstrated an immunomodulatory property that is closely related to the ADSC secretome. The secreted factors include hepatocyte growth factor, granulocyte and macrophage colony stimulating factors, interleukins-6, -7, -8 and -11, tumor necrosis factor-alpha, vascular endothelial growth factor, brain derived neurotrophic factor, nerve growth factor and adipokines [29]. Therefore, ADSCs may be an ideal cell source for transplantation and peripheral nerve regeneration.

In the present study, we developed an artificial nerve graft composed of CS/SF seeded with ADSCs and investigated whether enwrapping of the lesion site improves regeneration and recovery rates. The artificial nerve scaffold was used to regenerate a 10 mm surgically-induced sciatic nerve injury in a rat model. The clinical outcome was evaluated by various histological methods at 24 weeks post-surgery.

2 Materials and methods

2.1 Materials

Bombyx mori silk was purchased from Shibanyan Xinxing raw silk factory, Linzhou, Anyang, Henan, China. CS was obtained from Qingdao Haisheng Co., Qingdao, Shandong, China. The degree of deacetylation was estimated to be 93.5% using the 1H-NMR method and the viscosity-average relative molecular weight was 1.8×10^6 Da.

Trypsin and Dulbecco's modified Eagle medium/F-12 Ham nutrient mixture (DMEM/F-12) were purchased from Invitrogen. Collagenase type II was purchased from Merck. Cytosine-B-arabinoside hydrochloride (Ara-C), penicillin and streptomycin were purchased from Sigma. Human heregulin1-β1 Extracellular Domain (HRG1-β1 ECD) was from R&D system. Fetal bovine serum (FBS) was obtained from Hyclone. All the culture plates and clusters were from Costar. All other reagents were local products of analytical grade.

Primary antibodies employed for immunocytochemistry, including mouse-anti-S-100 protein antibody and rabbit anti-neurofilament H (200 kDa) antibody, were obtained from Millipore. Secondary antibodies including FITC goat anti-rabbit IgG (H + L) and TRITC goat anti-mouse IgG (H + L) were purchased from Invitrogen.

Postnatal Sprague-Dawley rats (either sex, 1–3 days old, for SC isolation) and adult Sprague-Dawley rats (male, 6–8 weeks old, for ADSCs isolation; female, 200–300 g,

for nerve regenerative surgery) were obtained from Beijing Haidian Experimental Animal Center. All animal experiments were carried out in accordance with the US National Institutes of Health Guide for the Care and Use of Laboratory Animals (NIH Publications No. 80-23) revised 1996 and approved by the Beijing Administration Committee of Experiment Animals.

2.2 Cell isolation and culture

Schwann cells were enriched from the sciatic nerves of postnatal Sprague-Dawley rats as described in our previous study [30]. The adipose tissue was purified from the testicular fat pads of adult Sprague-Dawley rats. Isolation of ADSCs was accomplished using a modification of published methods [31]. The obtained adipose tissues were washed with cold DMEM/F-12 medium and mechanically dissociated by scissors. After that, the adipose tissues were digested with collagenase type II for 40 min at 37°C and then dissociated carefully with pipettes. The suspension was filtered through 80-μm metal mesh and centrifuged to separate the floating adipocytes from stromal vascular fraction. The supernatant was discarded and cells in the stromal vascular fraction were re-suspended in DMEM/F-12 medium (containing 1% penicillin/streptomycin and 10% FBS) and seeded onto culture plates. 24 h later, the culture medium was changed to eliminate the non-adherent cells. Cells used in our experiments were passaged for 3–5 times.

2.3 Flow cytometry

Rat ADSCs within 3–5 passages after the initial plating of the primary culture were harvested, and then the cells were centrifuged and re-suspended in PBS. Each 1.5 ml tube was placed with 1×10^6 cells. Then the cells were washed twice with PBS, and incubated for 30 min on the ice with the following FITC-conjugated primary antibodies, including CD11b, CD31, CD45, CD44 and CD90. For control samples, nonspecific FITC-conjugated IgG was substituted for the primary antibodies and analyzed by BD FACSAria™ II Flow Cytometer (BD Biosciences, USA).

2.4 SF purification and concentration

The sericin coating of raw silk fiber from Bombyx mori cocoon was removed via degumming. In brief, 0.5% (w/v) sodium carbonate was dissolved and brought to 100°C. Raw silk was added at 1:100 (w/v) and heated for 1 h, followed by draining of the alkaline soap solution. The degummed silk was rinsed in running distilled water. After all the remaining sericin was removed completely, the washed silk was air-dried.

The degummed silk was then dissolved in calcium dichloride-ethanol solution (molar ratio, $CaCl_2$:H_2O:C_2H_5OH 1:8:2) at 80°C as described previously [32]. The solution was cooled and then dialyzed against the distilled water for 3 days. After vacuum filtration, the SF aqueous solution was stored at 4°C until use. The concentration of SF aqueous solution was determined by BCA protein assay kit (Pierce). The final SF concentration can be adjusted to meet the need by concentrating the solution at 40°C or diluting.

2.5 CS dissolution and blending with SF solution

CS solution was prepared by dissolving 3% (w/v) CS in 1.5% (w/v) acetic acid. The solution was filtered through a middle-pore-size nylon cloth (Hualu medical material company, Shandong, China) to remove insoluble substances. An equal volume of 10% (w/v) SF was added to the filtered CS solution to prepare a 50:50 blend ($V_{3\%CS}$:$V_{10\%SF}$ = 50:50) and allowed to mix for 15 min. The final blend was named 5CS/5SF, which was clear and homogeneous and stored at 4°C until use. In addition, 70:30 blends ($V_{3\%CS}$:$V_{10\%SF}$ = 70:30) were prepared in the similar manner (7CS/3SF).

2.6 Preparation of SF-CS blend film

The above blends were degassed and then cast into the wells of 24-well Costar tissue culture clusters (0.3 ml/well for 24-well cluster), and dried at 50°C for 48 h to form thin membrane substrates. After drying, the membranes were treated with methanol for 2 h, and then immersed into NH_4OH solution for 30 min. Finally, the film was washed with the distilled water until neutrality, and then air-dried. A pure CS membrane was processed with the same procedure as controls. For all membranes, their thickness was ~20 μm, which was measured by micrometer caliper.

2.7 Cell adhesion and proliferation on CS/SF blend films in vitro

SCs and ADSCs were used to evaluate the biocompatibility of the blended CS/SF films. Prior to cell culture assays, all tissue culture clusters were sterilized by exposure to UV light for 30 min. Two types of cells were routinely removed from tissue culture dishes, and were seeded on the pretreated tissue culture clusters obtained as described in Sect. 2.5. All substrates remained fully transparent, which allowed direct observation of cell morphology with an inverted phase contrast microscope. Cells cultured after 24 h were viewed using an inverted phase contrast microscope (Axiovert 10, Opton). Images from the

microscope were acquired using a CCD video camera (CCD color camera, Hitachi).

An MTT test was performed to quantify the cell viability. Briefly, cells were cultured for 1, 3, and 5 days, and 100 μl MTT (3-(4,5-dimethylthiazol-2-yl)-2, 5-diphenyltetrasodiuim bromide, 5 mg/ml, Amresco 0793) was added to each well and were incubated at 37°C for 4 h. Then, the MTT solution was removed and the insoluble blue formazan crystal was dissolved in dimethyl sulfoxide. 100 ml of solution from each well was aspirated and poured in a 96-well plate. The absorbance was measured at 570 nm using an ELISA reader (Bio-Rad Model 550, USA). In addition, MTT assay was performed on a directly counted cells serial (0.2×10^5, 0.4×10^5, 0.8×10^5, 1.6×10^5, 3.2×10^5, 6.4×10^5), and the absorbance values were plotted against the counted cell numbers to establish a standard calibration curve. Viable cell numbers were then determined from the standard curve based on their MTT absorbency. Cells numbers were represented as means ± standard deviation (SD).

2.8 Fabrication of CS/SF nerve conduit

CS/SF nerve conduit was prepared by the method as described previously with minor modification [33]. In brief, the blended solution was obtained and degassed as described in Sect. 2.4. Then the solution was injected gently into a homemade mold using a syringe, frozen in liquid nitrogen for 30 min, followed by lyophilization for 48 h. The dried samples were removed from the molds and treated in methanol for 2 h to crystallize the silk content. The methanol was then replaced with NH_4OH solution overnight to neutralize the acetic acid content. To remove the NH_4OH solution, the samples were rinsed several times using deionized water until the rinsing solution was neutral, and then equilibrated in 0.2 mol/l phosphate buffered saline solution (PBS, pH 7.4) for 30 min. The surface water of the samples was absorbed by filter paper and dried at room temperature, and then the mandrel was removed to produce a porous CS/SF conduit. CS nerve conduit was prepared as described above without modification.

2.9 Characterization of the silk fibroin-chitosan nerve conduit

2.9.1 Scanning electron microscopy (SEM)

The scaffolds were mounted on aluminium stumps and coated with gold in a sputtering device for 3 min at 15 mA under vacuum. The surface and cross-section morphologies of CS and SF-CS scaffolds were examined with a scanning electron microscope (KYKY-2800, Apparatus Factory, Chinese Academy of Sciences, Beijing, China) with an acceleration voltage of 20 kV.

2.9.2 Mechanical properties

The mechanical properties of the conduits were tested with a universal testing machine (AG-1, Shimadzu Co, Japan). All the samples were tested in a wet state after immersion in PBS for 24 h. Tensile strength was evaluated by applying a force parallel to the longitudinal axis of a conduit. Six replicates were included in each group.

To investigate the suture retention ability of the scaffolds, the tensile testing was performed by mimicking in vivo surgical procedures as described previously [34]. Briefly, the scaffold was sutured to epineuria between two stumps of goat common peroneal nerve obtained from a local abattoir with 8-0 nylon sutures at two opposite sites on both ends. At least seven knots were tied at the end of the each suture to prevent slippage. The two nerve stumps were clamped into the testing device, and force was applied parallel to the axis of the conduits at an extension speed of 10 mm/min until the suture pulled out of the testing scaffold or epineuria. The maximum load was recorded as the suture retention strength of the scaffolds. At least six samples were measure, and the average values were obtained.

2.9.3 Swelling index and expansion ratios measurements

Dried CS/SF and CS conduits were weighed and subsequently immersed in PBS, (pH 7.4) for 24 h. The mass of the swollen samples were measured after the surface water was removed with filter paper. The changes in inner diameter and wall thickness of the conduits were measured by a micrometer caliper. For each experimental value, five independent experiments were conducted. The swelling properties of the conduits were evaluated by the following parameters:

$$\mathrm{SI} = ((\mathrm{Ws} - \mathrm{Wd})/\mathrm{Wd}) \times 100\%, \quad (1)$$

$$\mathrm{T} = ((\mathrm{Hs} - \mathrm{Hd})/\mathrm{Hd}) \times 100\%, \quad (2)$$

$$\mathrm{D} = ((\mathrm{Ds} - \mathrm{Dd})/\mathrm{Dd}) \times 100\%, \quad (3)$$

where SI is the swelling index. Wd and Ws is the mass of the dried and swollen grafts; T is the increase in wall thickness of a conduit. Hd and Hs is the wall thickness of the dried and swollen grafts; D is the change in inner diameter of the conduit. Dd and Ds is the inner diameter of the dried and swollen grafts.

2.9.4 Cells loading of CS/SF conduits

Freeze-dried CS/SF conduits were sterilized with 70% ethanol immersion overnight, decontaminated by exposure

to ultraviolet irradiation for 1 h, and incubated in sterile PBS prior to in vitro cell seeding. Conduits of 12 mm in length were injected with 200 µl DMEM/F12 culture medium alone in the CS/SF group and with an equal volume of cell suspension containing 1×10^6 cell/ml SCs in the SC-7CS/3SF group, and 1×10^6 cell/ml ADSCs in the ADSC-7CS/3SF group. Conduits were incubated in 5% CO_2 incubator at 37°C for 3 h, after which the overlying medium or cell suspension was aspirated. The conduits were then dipped into DMEM/F12 culture medium and incubated under standard culture condition for 48 h. When conduits were transferred to the operative field for surgical engraftment, they were moved to a sterile six-well plate and washed gently in two 1 ml aliquots of PBS to remove any non-adherent cells or medium.

In order to examine whether grafted cells were survived, cell viability and proliferation was determined by using CCK-8. Briefly, conduits of 2 mm in length were injected with 30 µl DMEM/F12 culture medium alone in the CS/SF group and with an equal volume of cell suspension containing 1×10^5 cell/ml SCs in the SC-7CS/3SF group, and 1×10^5 cell/ml ADSCs in the ADSC-7CS/3SF group. Conduits were incubated in 5% CO2 incubator at 37°C for 3 h, after which the overlying medium or cell suspension was aspirated. The cell-loaded conduits were cultured DMEM/F 12 medium and incubated under standard culture in 96-well plate. After 1, 3, 5, 7 days, 10 µl CCK-8 was added to each well. Aftet incubation at 37°C for 4 h, the absorbance of WST-8 [2-(2-methoxy-4-nitrophenyl)-3-(4-nitrophenyl)-5-(2,4-disulfophenyl)-2H-tetrazolium, monosodium salt] in each well at 450 nm was measured with an ELISA reader (Bio-Rad Model 550, USA).

2.9.5 Surgical procedures

Based on the results of the above physical and biological properties of the scaffolds, 7CS/3SF scaffold was selected to regenerate the sciatic nerve across a 10-mm long surgically induced sciatic nerve injury in a rat model. Briefly, 32 female Sprague-Dawley rats (200–230 g) were used to evaluate the nerve regeneration in 7CS/3SF scaffold. The animals were randomly divided into four groups: (1) the SC-7CS/3SF scaffold group ($n = 8$); (2) ADSC-7CS/3SF scaffold group ($n = 8$); (3) 7CS/3SF scaffold group ($n = 8$); (4) the non-grafted rats as a negative control group ($n = 8$). For the surgical procedures, the animals were anesthetized by administering 10% chloral hydrate (0.35 ml/100 g) intraperitoneally (i.p.) and the left sciatic nerve was exposed through a skin incision extending from the greater trochanter to the mid-thigh followed by splitting the overlying gluteal muscle. The nerve injured model was performed by half sectioning the exposed sciatic nerve through a fine scissor cut every 2 mm within 1 cm as shown in Fig. 1c. The injured sciatic nerve was then enwrapped by the splitted nerve conduits with 10-0 nylon sutures as shown in Fig. 1e. For the negative control group, the nerve defect was left uncovered. Finally the muscle layer was anastomosed with 4-0 nylon sutures, and the skin was closed with 2-0 silk sutures.

2.9.6 General observation

After surgery, all rats were housed and fed routinely, and monitored for changes in their appearance, hind limb movements, healing of the surgical wounds, and ulcer

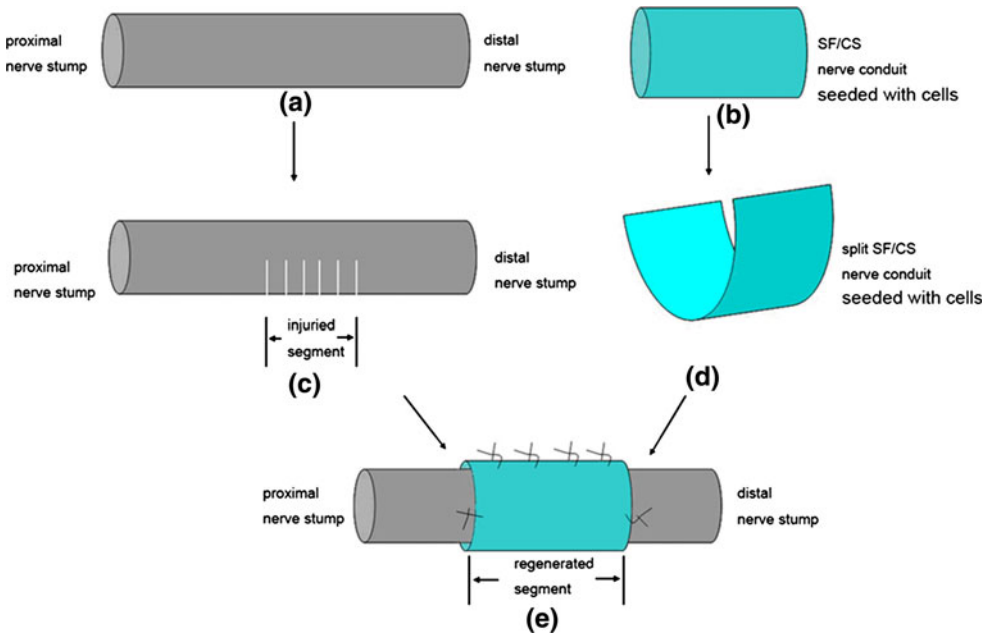

Fig. 1 A schematic illustration of the nerve injured model and the surgical procedures

formation in the foot. At 24 weeks post-operatively, the rat was held by the tail and lowered toward the cage, and then pulling it upward when the animal gripped the grid. The posture of each rat was recorded by the aid of photos at 24 weeks after surgery.

2.9.7 Functional evaluation

In order to assess the functional nerve recovery, walking track analysis was performed on animals in the four different groups at 12 and 24 weeks after surgery, as previously described [35]. Briefly, footprints were recorded by painting the rat hind paws with China ink and have them walk along a 40 × 8 cm track on white paper, with a dark shelter at the end. Several measurements were taken from the footprints: (1) distance from the heel to the third toe, the print length (PL); (2) distance from the first to the fifth toe, the toe spread (TS); and (3) distance from the second to the fourth toe, the intermediary toe spread (ITS). All the above measurements were taken from the experimental (E) and normal (N) sides. Footprints for measurements were chosen at the time of walking based on clarity and completeness at a point when the rat was walking briskly. Sciatic functional index (SFI) was calculated according to the following equation:

$$\begin{aligned}\mathrm{SFI} = &-38.3(\mathrm{EPL}-\mathrm{NPL})/\mathrm{NPL} \\ &+ 109.5(\mathrm{ETS}-\mathrm{NTS})/\mathrm{NTS} \\ &+ 13.3(\mathrm{EITS}-\mathrm{NITS})/\mathrm{NITS} - 8.8 \end{aligned} \quad (4)$$

For SFI, an index score of 0 is considered normal and an index of −100 indicates total impairment of the sciatic nerve. When no footprints were measurable, the index score of −100 was given. In each walking track, three footprints were analyzed by a single observer, and the average of the measurements was used in SFI calculations.

2.10 Histological assessment

Following walking track analysis at week 24 postoperatively, the nerve grafts and gastrocnemius muscles were harvested from the operated and contralateral sides for the following experiments.

2.10.1 Muscle mass

Recovery assessment was also indexed as the weight ratio of the gastrocnemius muscle. The gastrocnemius muscles dissected from the operated and contralateral unoperated sides were weighed damp. A conservation muscle-mass ratio, given in percentages, was calculated for each animal by dividing the muscle mass of the operated side by those of the unoperated side. All counts were made by two independent observers unaware of the analyzed group.

2.10.2 Immunohistochemistry

The nerve specimens in each group were fixed in buffered 4% paraformaldehyde for 24 h, and transferred to the 30% sucrose in 0.1 M PBS, and then cut into 15 μm thick transverse sections on a cryostat. Sections were blocked in 5% normal goat serum for 30 min at room temperature, and allowed to incubate with rabbit anti-neurofilament 200 kD polyclonal antibody (1:100) and mouse anti-S-100 protein monoclonal antibody (1:100), at room temperature for 1 h. The sections were washed three times with PBS and further reacted with the corresponding secondary antibodies, a FITC goat anti-rabbit IgG (1:50) and a TRITC goat anti-mouse IgG (1:50), at room temperature for 2 h. After a second rinsing step with PBS/Tween, sections were mounted with antifade solution. Labeled sections were examined with fluorescence microscopy. The nerve specimens obtained from the unoperated site were served as a positive control. The images were digitally recorded and processed with Image-Pro Plus.

2.10.3 Electron microscopy observation

For the histological analysis, the regenerated nerve specimens were fixed with pre-cooled 2.5% glutaraldehyde in 0.1 M PBS for 2 h and post-fixed in 1% osmium tetraoxide solution for 1 h. Then they were dehydrated stepwise in increasing concentrations of ethanol, and embedded in Epon 812 epoxy resin. The mid-portions of the specimens were cut into semi-thin cross-sections of 1 μm thickness with an ultramicrotome (EM UC6, Leica, Germany), and stained with toluidine blue for measuring the cross-sectional area of the total nerve trunk area by light microscopy. The nerve specimens obtained from the unoperated site were served as a positive control.

To observe more detailed axon and myelin sheath regeneration inside the tubes, the specimens were also cut into ultra-thin sections with 70 nm thickness. The sections were stained with lead citrate and uranyl acetate, and then examined by a transmission electron microscopy (TEM; H-7650, Hitachi, Japan). The nerve specimens from the unoperated site were used as a positive control for nerve histological analysis. The electron microscopic images from 8 random fields of each nerve section were selected and analyzed by Image-Pro Plus software to obtain morphometric parameters. In brief, for each selected field, individual myelinated nerve fibers were counted, and myelinated fiber diameter (D) and axon diameter (d) were measured. These data were used to calculate myelin thickness ((D − d)/2) and g-ratio (d/D). The g-ratio of an axon is a measure of myelin thickness calculated by dividing the axonal diameter by the total diameter of axon plus myelin sheath. The myelinated fiber density was

determined by examing the ratio of the myelinated fibers/total area analyzed.

2.11 Statistics

All data were expressed in the text as mean ± SD. For comparison of quantitative measures, the values were subjected to statistical analysis using Students *t*-test, and statistical significance was accepted at the 0.05 confidence level.

3 Results

3.1 ADSCs identification

Flow cytometric analysis of passage 3–5 rat ADSCs revealed that the cells were CD44 and CD90 positive, and CD11b, CD31 and CD45 negative (Fig. 2). This result was consistent with previous reports [36] that revealed ADSCs express CD90 and lack hematopoietic lineage markers CD11b and CD45.

3.2 Cell adhesion and proliferation on CS/SF blended films in vitro

SCs and ADSCs morphologies and adhesion on CS alone and two blended films are shown in Fig. 3. After 24 h, SCs on 7CS/3SF and 5CS/5SF films showed higher adhesion compared with those on CS control. ADSCs adhesion to these films showed a similar pattern. Furthermore, many of SCs on the CS film maintained a spherical shape and only small number of SCs were bipolar. On the 7CS/3SF and 5CS/5SF films, extensions were observed from most cells that were characterized as phase-bright, spindle-shaped, bipolar or infrequent tripolar cells with low cytoplasm to nuclei ratios.

MTT assays were performed to assess cell proliferation on CS and CS/SF blended films. Equal cell numbers were seeded onto CS and blend films that contained various SF concentrations. Figure 4 shows the proliferation rates of SCs and ADSCs cultured on CS and blend films at days 1, 3 and 5. At day 1 in culture, SCs on 7CS/3SF and 5CS/5SF films demonstrated significantly higher SCs proliferation compared with those on the CS control. At days 3 and 5, 7CS/3SF and 5CS/5SF films maintained higher SCs proliferation compared with those on the CS control. ADSC proliferation demonstrated a similar pattern with an exception of the proliferation rate on the CS control did not decrease on day 5.

3.3 Characterization of the CS/SF nerve conduit

3.3.1 Scanning electron microscopy (SEM)

After scaffolds were treated with methanol and sodium hydroxide, the sheet structure remained but was more compact (Fig. 5a–c). All three conduit types possessed a well defined and integrated sheet structure, and 7CS/3SF is much superior. This sheet formation is the first step towards mimicking the layered basement membrane

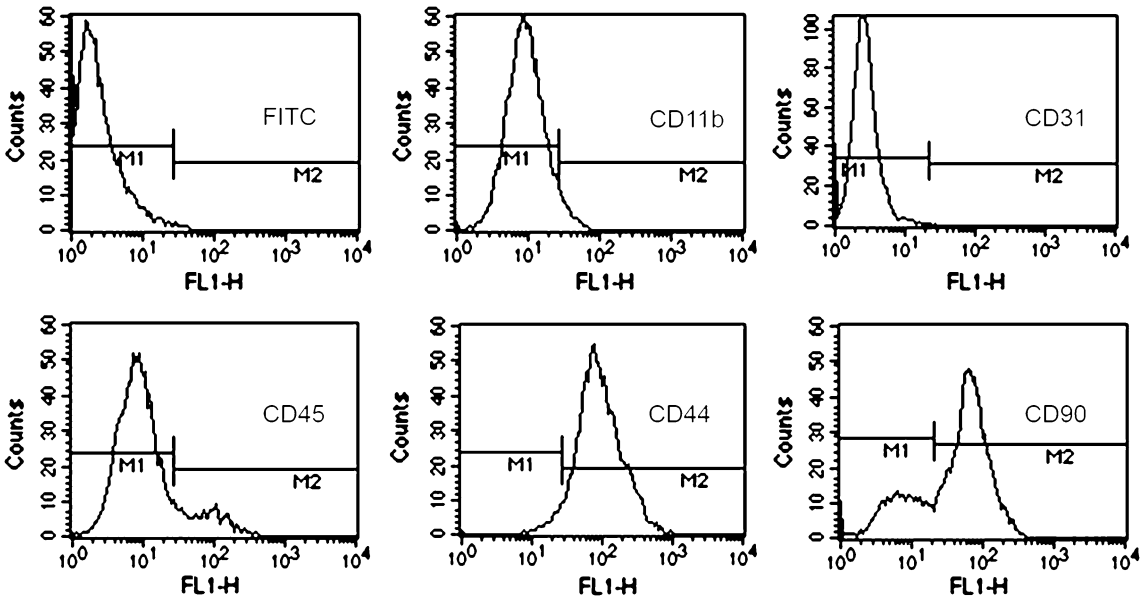

Fig. 2 Flow cytometric analysis of rat ADSCs. Results shows that rat ADSCs don't express CD11b, CD31 and CD45, but express C44, and CD90

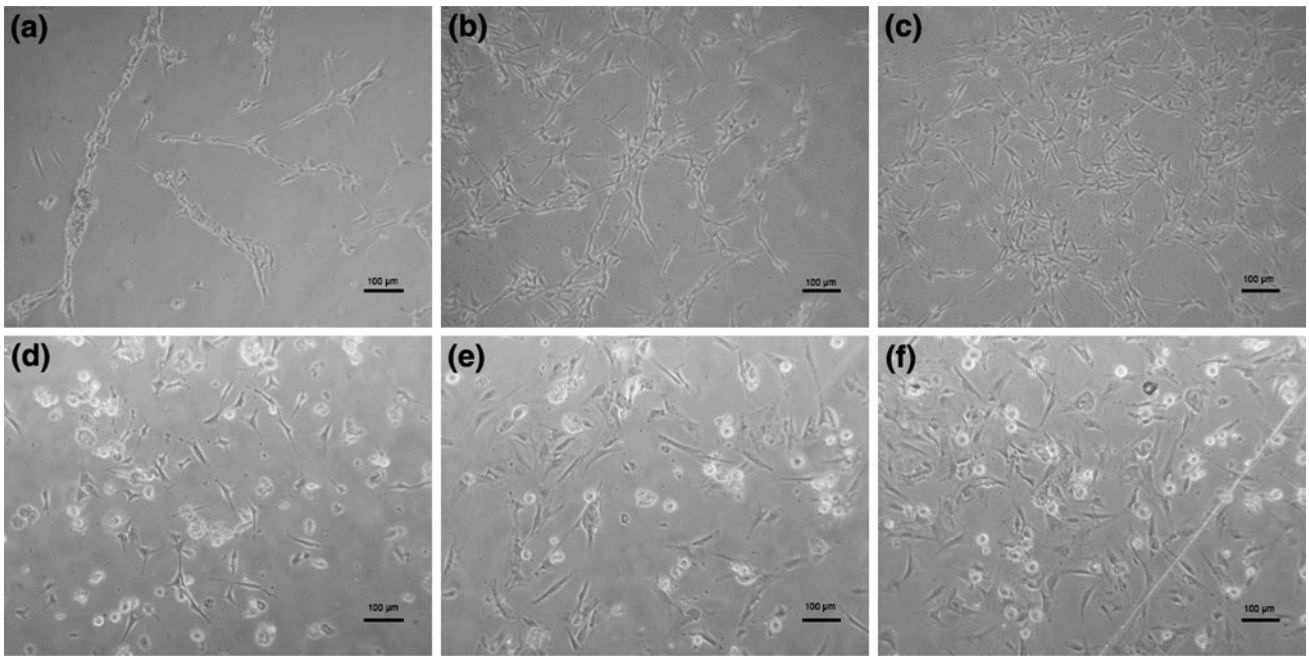

Fig. 3 Phase-contrast photomicrograph of SCs and ADSCs 24 h after cells seeding on CS and CS/SF blend films. **a–c** SCs on CS, 7CS/3SF and 5CS/5SF film, respectively; **d–f** ADSCs on CS, 7CS/3SF and 5CS/5SF film, respectively. (*Scale bar* 100 μm)

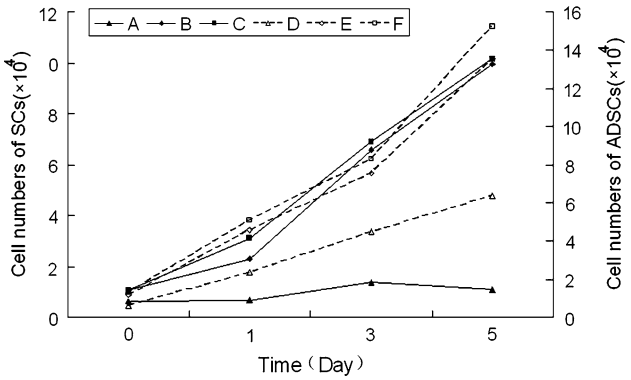

Fig. 4 Proliferation of rat SCs and ADSCs on CS and CS/SF blend films. *A–C* SCs on CS, 7CS/3SF and 5CS/5SF film, respectively; (*D–F*) ADSCs on CS, 7CS/3SF and 5CS/5SF film, respectively

structure. In addition, fiber-like morphology was observed on the interior surface of the conduits with increasing of SF concentration (Fig. 5d–f).

3.3.2 Mechanical properties

Appropriate mechanical properties are required for nerve scaffolds to remain intact during a suture process and provide a temporary mechanical support sufficient to withstand in vivo forces exerted by the surrounding tissues. In addition, a space must be maintained for tissue redevelopment. Conduit tensile strengths are shown in Table 1. The scaffold elastic modulus, tensile strength and elongation-at-break of the scaffold decreased with increasing of SF concentrations. An elastic modulus decrease may improve the flexibility of the blended scaffold for nerve regeneration. However, the tensile strength and elongation-at break of the 5CS/5SF scaffold make it too fragile for medical implantation. Moreover, 5CS/5SF conduits were brittle during fabrication compared with those of CS and 7CS/3SF conduits (Fig. 6).

To determine whether scaffolds were too fragile for implantation, tensile analysis was performed by mimicking in vivo surgical procedures. Suture retention strengths of CS and 7CS/3SF conduits were high enough to resist the applied extension force (the epineurium was divulsed at ~2 N, Table 2), while the 5CS/5SF conduit was physically weak (the conduit was divulsed at ~1.42 N while the epineurium remained intact, Table 2). These results were consistent with our observation and their own mechanical properties. Therefore, the 7CS/3SF conduit may be an appropriate scaffold for the treatment of peripheral nerve injuries.

3.3.3 Swelling index and expansion ratios measurements

Swelling properties of CS and blended scaffolds are listed in Table 3. The swelling index, diameter change and wall thickness decreased with an increasing SF concentration. CS contains primary amines and hydroxyl groups that result in the polymer being hydrophilic. SF is a fibrous protein that does not significantly swell. Therefore, the

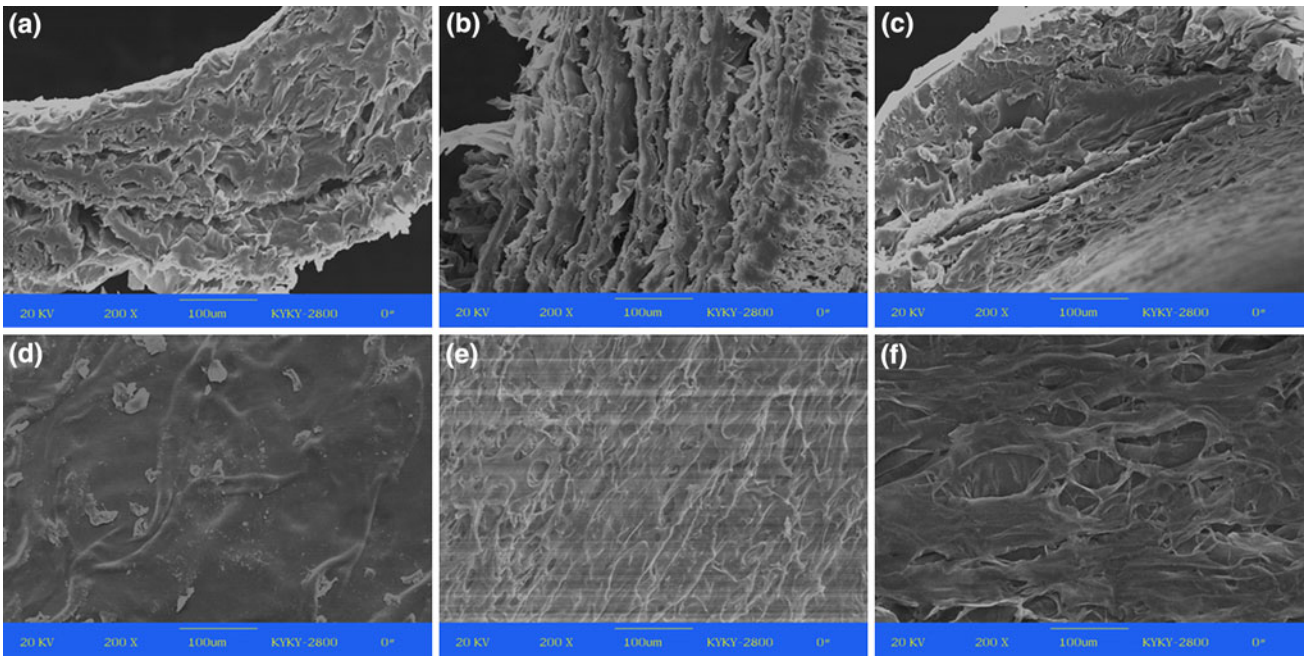

Fig. 5 SEM images of porous CS and CS/SF conduit. **a–c** Transection view of CS, 7CS/3SF and 5CS/5SF conduit, respectively; **d–f** Interior surface of CS, 7CS/3SF and 5CS/5SF conduit, respectively (*Scale bar* 100 μm)

Table 1 Mechanical properties of CS and CS/SF conduits

Sample name	Elastic modulus (MPa)	Tensile strength (MPa)	Elongation-at-break (%)
CS	6.8 ± 0.5	4.7 ± 0.4	62 ± 8.7
7CS/3SF	5.3 ± 0.2	3.1 ± 0.7	56 ± 7.4
5CS/5SF	3.4 ± 0.3	2.1 ± 0.5	33 ± 4.8

Values are mean ± SD, $n = 6$

Table 2 The suture retention strength of the scaffolds

Sample name	Maximum load (N)	Result description
CS	2.18 ± 0.23	The epineuria were divulsed
7CS/3SF	1.96 ± 0.25	The epineuria were divulsed
5CS/5SF	1.42 ± 0.18	The scaffolds were divulsed

Values are mean ± SD, $n = 6$

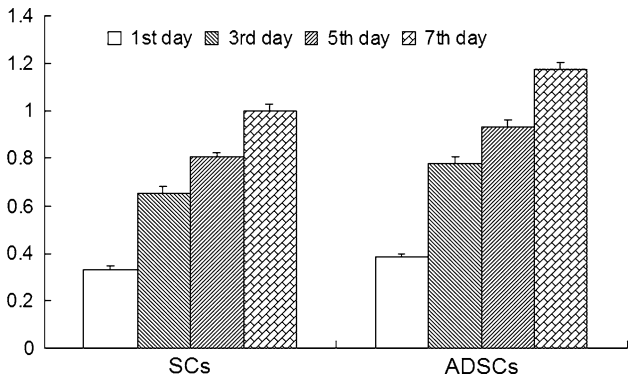

Fig. 6 Cell proliferation analysis of SCs and ADSCs cultured on 7CS/3SF on day 1, 3, 5, 7

swelling changes are probably due to the properties of CS. To produce an optimal scaffold, CS and SF needed to be blended at a suitable proportion.

Table 3 Swelling properties of CS and CS/SF conduits

Parameters	Value (%)		
	CS	7CS/3SF	5CS/5SF
SI	423 ± 35	348 ± 39	328 ± 57
T	128 ± 26	118 ± 34	115 ± 27
D	−13 ± 3	−11 ± 2	−11 ± 1

Values are mean ± SD, $n = 5$

3.4 Cell viability and proliferation on 7CS/3SF conduit

To examine grafted cell survival, viability and proliferation was determined by CCK-8. SCs and ADSCs proliferation rates on 7CS/3SF conduits from day 1 to 7 are shown in Fig. 8. Both SCs and ADSCs proliferated well on 7CS/3SF scaffolds with a 1.86-fold increase in SCs and 2.14-fold increase in ADSCs at day 7. These results indicated that

SCs and ADSCs not only survive but also proliferate efficiently after seeding on a 7CS/3SF conduit.

3.5 General observation

Complications related to surgical procedures did not occur. Wounded tissues spontaneously healed and there were no trophic ulcers on operated limbs or experimental animal fatalities. Following surgery, locomotor functions were completely absent in operated limbs. Palms on the operated side of rats could not touch the ground while walking. A small number of animals in the negative control group had shown a tendency to auto-mutilate treated digits and some mutilated the entire forefoot. After 24 weeks, both the SCs-7CS/3SF and ADSCs-7CS/3SF grafted rats were able to grasp a grid (Fig. 7a, b) and coordinate their movement with each other. Operated limb strengths appeared approximately equal to contralateral limbs. Locomotor recovery of the 7CS/3SF scaffold group was less than that of the ADSCs-7CS/3SF scaffold group (Fig. 7c), but more than that of the negative control (Fig. 7d). In the negative control, operated hind limbs demonstrated limping, gastrocnemius muscle atrophy, load-bearing incapacity and uncoordinated motion with unoperated hind limbs (Fig. 7c). Neither scaffold dislocation nor neuroma formation was observed in grafted rats. However, there was loose tissue in the injured segment of the negative control (Fig. 8). Serious adhesion of the injured segment to the epimysium of the underlying musculature was also observed.

3.6 Functional evaluation

The SFI value is one of the crucial indexes that evaluate the recovery of hind limb sensory and motor function, and it varies from 0 to −100, with 0 corresponding to normal function and −100 to complete dysfunction. In order to avoid the adverse impact of gait analyses and motor performance caused by the loss of a foot, rats with mutilated feet were removed from the analyses. Figure 9 displays the changes in the SFI value of the four groups during 24 weeks post-nerve injury. The improvement in mean SFI values (SC-7CS/3SF scaffold group: −43.6; ADSC-7CS/3SF scaffold group: −41.4; 7CS/3SF scaffold group: −55.2) were observed from the twelfth week after transplantation, indicating that some regenerated axons have passed through the nerve graft and eventually into the target organ. Recovery of nerve function was also detected in the negative control group 24 weeks after surgery (SFI values: −62.2), but the extent was the lowest compared with other grafted groups. The mean SFI showed no significant difference between SC-7CS/3SF and ADSC-7CS/3SF scaffold group 24 weeks post surgery (SC-7CS/3SF scaffold group: −22.3; ADSC-7CS/3SF scaffold group: −23.5), while the value of the 7CS/3SF scaffold group followed behind (7CS/3SF scaffold group: −36.4).

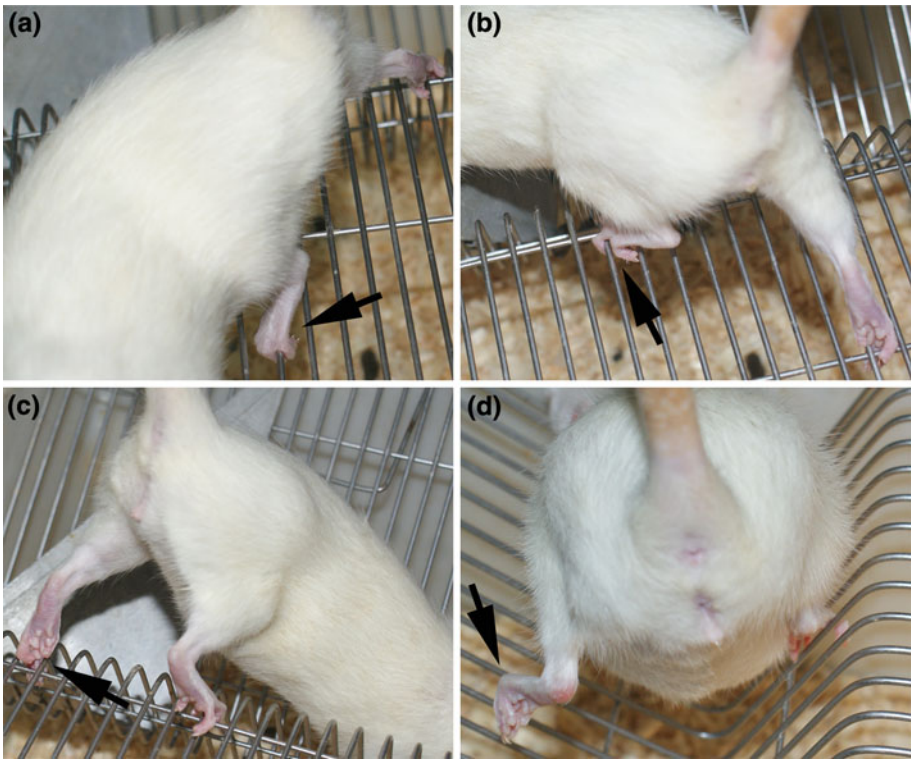

Fig. 7 Photographs demonstrating locomotion functions of the operated hind limb of rats at 24 weeks post-operatively in SC-7CS/3SF scaffold group (**a**), ADSC-7CS/3SF scaffold group (**b**), 7CS/3SF scaffold group (**c**) and the negative control group (**d**)

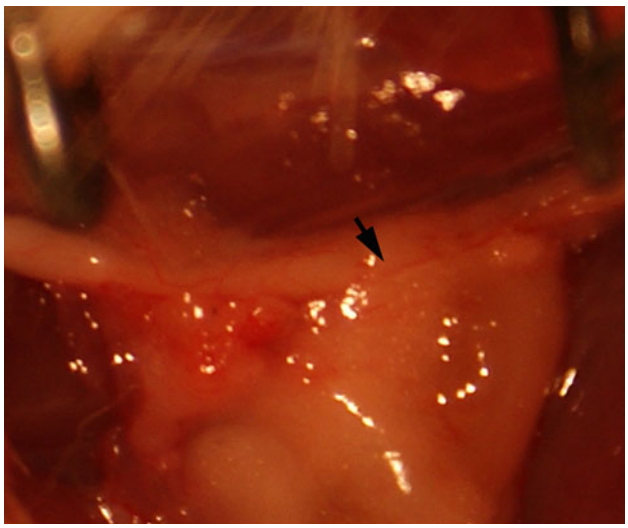

Fig. 8 Gross view of the regenerated nerve 24 weeks after injury in the negative control group. Serious adhesion of the injured segment to the epimysium of the underlying musculature was also observed

The statistical analysis revealed that the recovery of nerve function was significantly different between ADSC-7CS/3SF scaffold group and the 7CS/3SF scaffold group, and the latter were far superior to the negative groups.

3.7 Histological assessment

3.7.1 Muscle mass

The gastrocnemius muscles weight ratio, defined as the ratio of muscle wet weight of the operated side to the contralateral non-operated side, is more reliable than that of weighing the wet muscle itself. We found that 24 weeks after surgery, the mean wet weight ratio of the gastrocnemius for the ADSC-7CS/3SF scaffold group was similar to that for the SC-7CS/3SF scaffold group, but significantly higher than that for the 7CS/3SF scaffold group and the negative control group (Fig. 10), which indicated that ADSC-7CS/3SF graft greatly enhances the sciatic nerve regeneration process, since the relative preservation of muscle weight closely reflects the degree of muscle innervation.

3.7.2 Immunohistochemistry

At 24 weeks after nerve injury, double immunostaining with anti-NF200 and anti-S100 was performed to the distal portion of the sciatic nerves from the different groups. Numerous NF200 immunopositive nerve axons were seen in all the groups. NF200 and S100 immunopositive nerve axons in nerves of the unoperated site, SC-7CS/3SF scaffold group, ADSC-7CS/3SF scaffold group and 7CS/3SF scaffold group were arranged more evenly and densely (Fig. 11a3, b3, c3, d3). A large number of well-myelinated axons with larger diameter were observed in both SC-7CS/3SF and ADSC-7CS/3SF scaffold group in comparison to those in 7CS/3SF scaffold group, which indicated that ADSCs were beneficial as a cell therapy for peripheral nerve regeneration. The density of both NF200 and S100 immunopositive areas in the negative control group was greatly decreased as compared to all other groups (Fig. 11e3), which suggested that the CS/SF scaffold can mechanically block the invasion of scar tissue into the lesional area, and serve as a delivery vehicle for ADSCs.

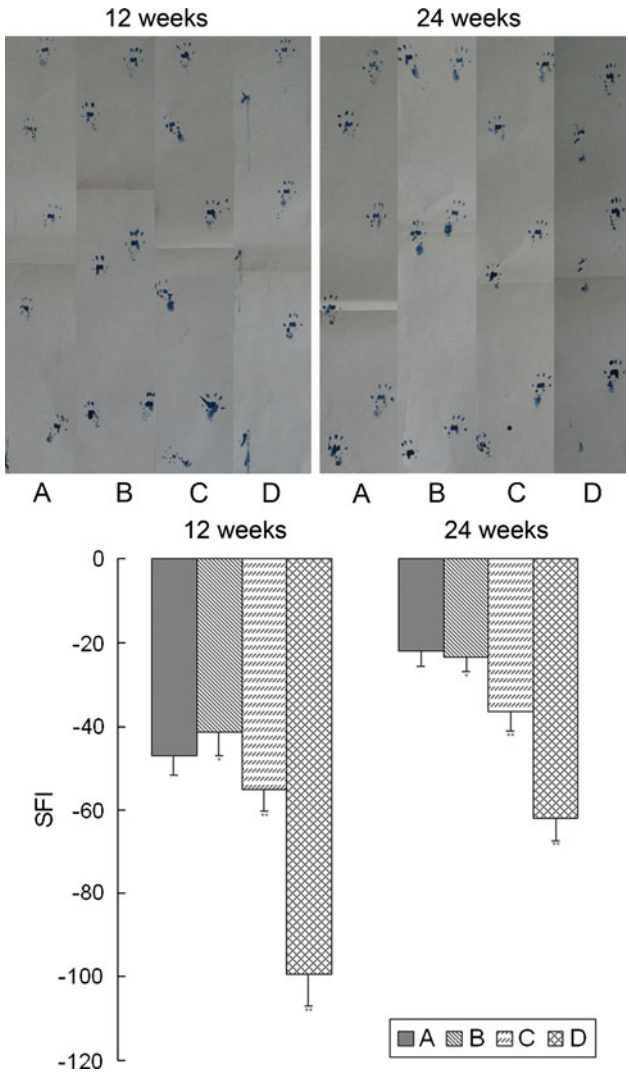

Fig. 9 Functional recovery after surgically sciatic nerve injury using walking track analysis. Measurements made from walking track prints were then submitted to SFI. *A* SC-7CS/3SF scaffold group; (*B*) ADSC-7CS/3SF scaffold group; (*C*) 7CS/3SF scaffold group; (*D*) negative control group. *$P < 0.05$ versus SC-7CS/3SF scaffold group; **$P < 0.05$ versus ADSC-7CS/3SF scaffold group

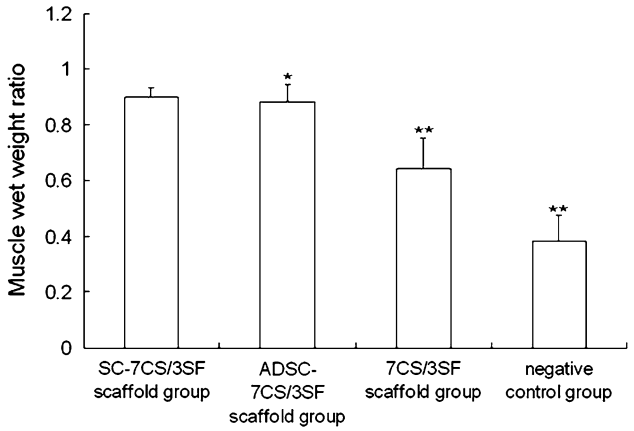

Fig. 10 Muscle wet weight ratio of the gastrocnemius muscle of the operated to contralateral hind limb after 24 weeks indicates a significantly reinnervation in ADSC-7CS/3SF scaffold group versus 7CS/3SF scaffold group and the negative control group. *$P < 0.05$ versus SC-7CS/3SF scaffold group; **$P < 0.05$ versus ADSC-7CS/3SF scaffold group

3.7.3 Histological observation

Transverse semi-thin sections of sciatic nerves from the middle portion of the injured sites were analyzed by Toluidine blue staining 24 weeks after surgery. Figure 12 shows the histological appearance of the nerve specimens from the unoperated site cross section compared with that of other regenerated nerve fibers. Regenerated nerve fibers in ADSC-7CS/3SF scaffold group and SC-7CS/3SF scaffold group were organized in microfascicles, which were similar to positive control nerve fibers, but much larger compared with those of the 7CS/3SF scaffold group and the negative control group. The formation of blood vessels was also observed (Fig. 12). Vascular tissue was increased in the negative control compared with that of the grafted groups.

Ultra-thin sections were also observed under transmission electron microscope. Results revealed the morphological features of the regenerated sciatic nerve in different groups at 24 weeks after nerve injury. As shown in Fig. 13a, myelinated axons were surrounded by thick and dark myelin sheath within the nerve specimens from the unoperated site (1.17 ± 0.02 μm). In the ADSC-7CS/3SF scaffold group, the myelinated axons were surrounded by a clear, thick, and electron-dense myelin sheath. The thickness of their myelin sheaths were similar to that of SC-7CS/3SF scaffold group (Fig. 13b, c, ADSC-7CS/3SF scaffold group, 0.75 ± 0.03 μm; SC-7CS/3SF scaffold group, 0.84 ± 0.05 μm, Table 4), but thicker than the 7CS/3SF scaffold group (Fig. 13d, 7CS/3SF scaffold group, 0.53 ± 0.07 μm, Table 4). The thickness of the myelin sheaths in the negative control group was the thinnest (Fig. 13e, 0.36 ± 0.13 μm, Table 4).

The statistical analysis revealed that the numbers of myelinated axons in the ADSC-7CS/3SF scaffold group were 18429 ± 3125/mm^2 (Table 4), which was similar to that of the SC-7CS/3SF scaffold group (15983 ± 1024/mm^2, Table 4), but significantly less than that of 7CS/3SF scaffold group (28800 ± 5286/mm^2, Table 4). The numbers of myelinated axons of the nerve specimens from the unoperated site were 12488 ± 943/mm^2. Myelinated axon diameter was significantly larger in ADSC-7CS/3SF scaffold group (5.80 ± 0.45 μm) compared with the other two operated groups (7CS/3SF scaffold group, 4.65 ± 0.31 μm; negative control group, 3.01 ± 0.37 μm, Table 4). The g-ratio is 0.73 ± 0.04 in the ADSC-7CS/3SF scaffold group, which is much smaller than that of the negative control group (0.83 ± 0.03).

The diameter of myelinated nerve fiber at the middle sciatic nerve portion was measured and the diameter distribution was plotted (Fig. 14). In the ADSC-7CS/3SF scaffold group, myelinated fibers 5–6 μm in diameter were as much as 35.2% of the whole population, and those 2–7 μm in diameter accounted for the majority (about 85.5% of the population). The diameter distribution of the ADSC-7CS/3SF scaffold group had a peak at around 5–6 μm, which was similar to that of the SC-7CS/3SF scaffold group. The distribution pattern in the 7CS/3SF scaffold group and negative control group was much more different from that in the ADSC-7CS/3SF scaffold group and the myelinated nerve fiber diameter in these two groups were smaller than that of the ADSC-7CS/3SF scaffold group. The diameter distribution of the positive control specimens had a peak at 6–7 μm.

4 Discussion

The aim of this study was to evaluate whether the local enwrapping of the lesion site with CS/SF scaffold seeded with ADSCs could improve the microenvironment of the injured sciatic nerve. Subsequently, we investigated whether this technique could induce axonal regeneration and locomotor functional recovery in the injured hind limbs of the experimental rats. The most significant findings in our study are summarized as follows: (1) with ADSCs-7CS/3SF scaffold enwrapping technique, regenerated nerve fibers entered the scaffold, traversed the lesioned area, and reentered the distal portion of the sciatic nerve. This observation was similar to the results of SC-7CS/3SF scaffold, which indicated that ADSCs use in cell therapy is advantageous for peripheral nerve regeneration; (2) the CS/SF scaffold may mechanically block the invasion of scar tissue into the lesional area (7CS/3SF scaffold group versus negative control group), and serve as a delivery vehicle for ADSCs in a rat sciatic nerve injury model (ADSCs-7CS/3SF scaffold

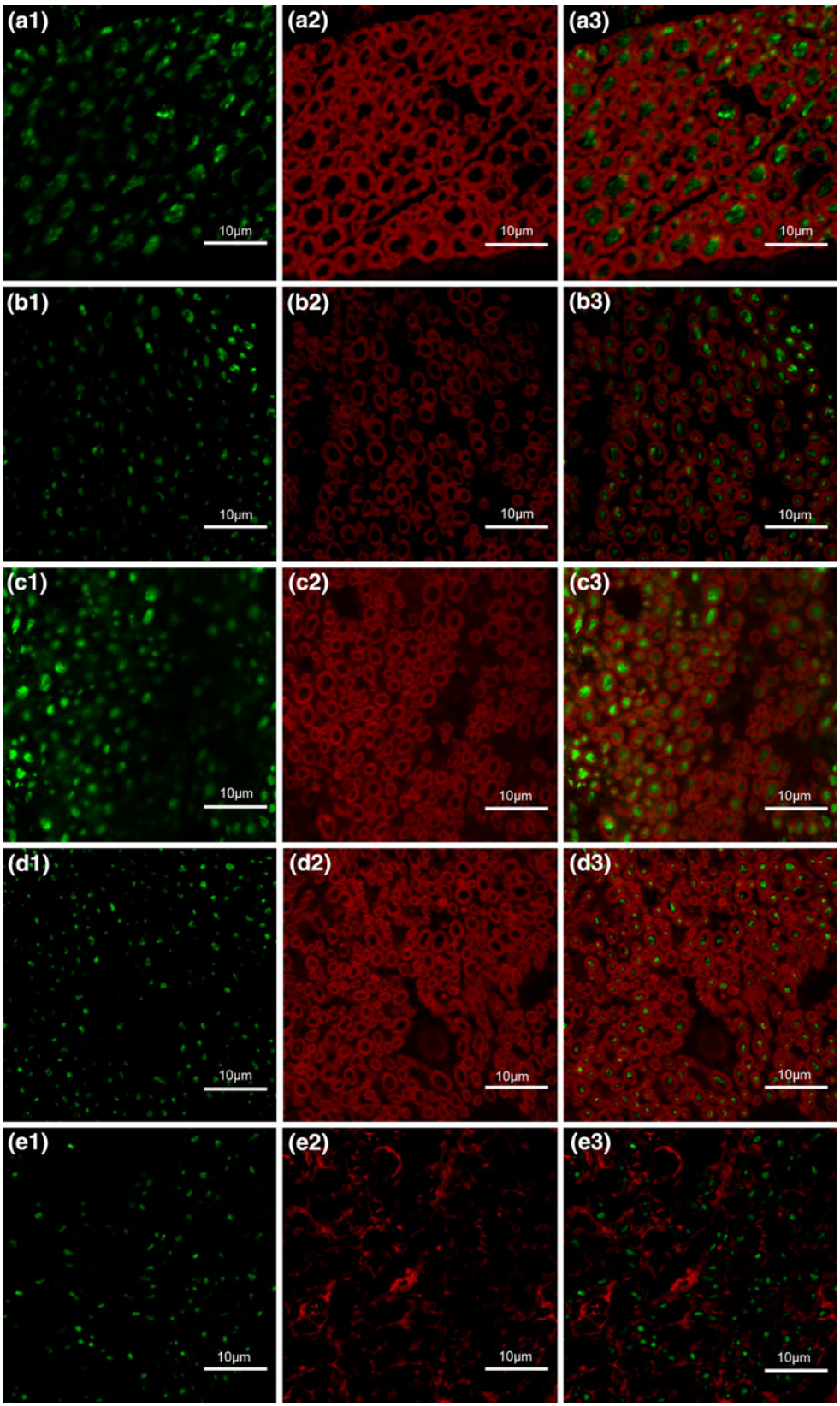

Fig. 11 Light micrographs following double-staining for NF-200 (a1–d1, *green*) and S-100 (a2–d2, *red*) (*merged* in a3–d3) on the transverse-sectioned distal portion of the regenerated segment in positive control (a1–a3), SC-7CS/3SF scaffold group (b1–b3), ADSC-7CS/3SF scaffold group (c1–c3), 7CS/3SF scaffold group (d1–d3), and negative control group (e1–e3), respectively (*Scale bar* 10 μm)

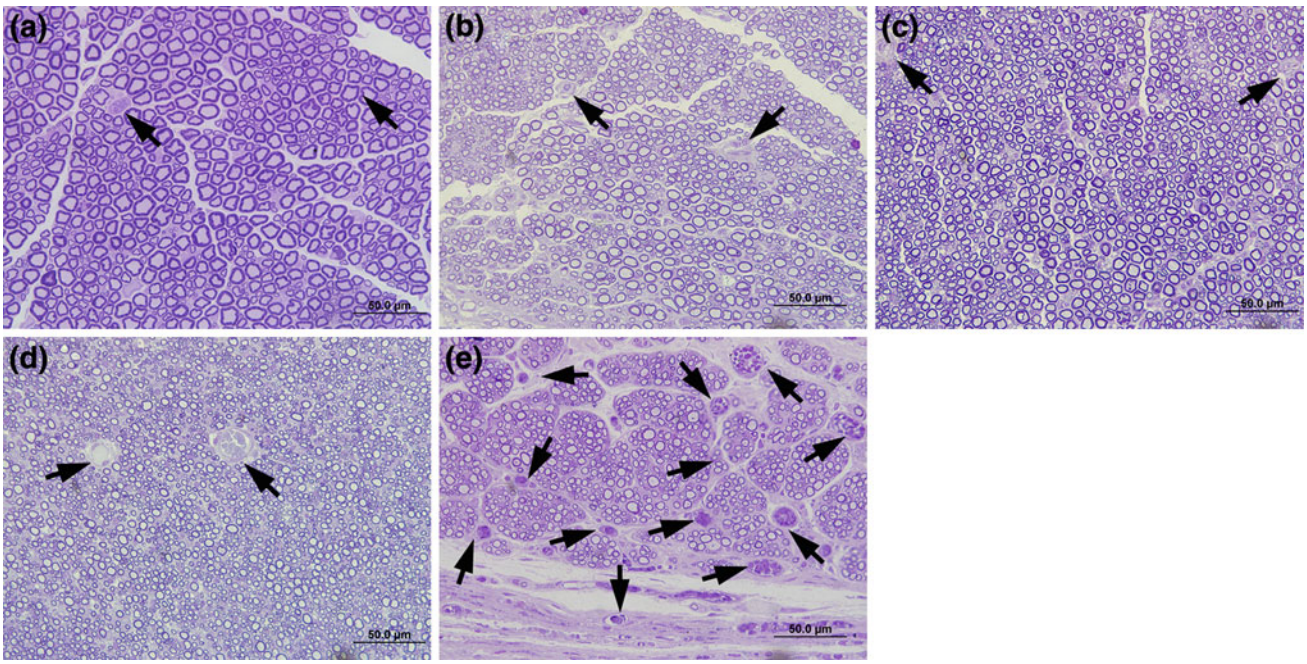

Fig. 12 Light micrographs following Toluidine blue staining on transverse-sectioned portion of middle sciatic nerve portion in positive control (**a**), SC-7CS/3SF scaffold group (**b**), ADSC-7CS/3SF scaffold group (**c**), 7CS/3SF scaffold group (**d**), and negative control group (e), respectively (*Scale bar* 50 μm). *Arrows* indicate the blood vessels

group versus 7CS/3SF scaffold group); (3) reconstruction of the injured sciatic nerve was significantly enhanced with restoration of nerve continuity and function recovery. In addition, target skeletal muscle was extensively reinnervated in the ADSC-7CS/3SF scaffold group versus 7CS/3SF scaffold and the negative control group.

Peripheral nerve injury is commonly classified as two schemes, Seddon and Sunderland. Seddon classified nerve injuries include neurapraxia, axonotmesis and neurotmesis [37]. Sunderland recognizes five degrees of nerve injury: (1) segmental demyelination; (2) the axon severed but endoneurium intact; (3) continuity loss of axons and endoneurial tubes; (4) continuity loss of axons, endoneurial tubes, perineurium and fasciculi but the epineurium intact; (5) the entire nerve trunk is totally transected [38]. Sunderland's first, second and fifth degree lesions correspond to Seddon's classification of neurapraxia, axonotmesis and neurotmesis. Reinnervation does not occur in fourth and fifth degree lesions without surgical repair. In our rat model of sciatic nerve injury, we induced a half continuity loss of axons, endoneurial tubes, perineurium, fasciculi and epineurium, which may be classed as neurotmesis or a Sunderland lesion between the fourth and fifth degrees. Without a surgical repair, scar tissue blocks regenerating axons from reaching the distal stump. Nerve function recovery was rarely detected in the negative control group even 24 weeks after surgery. Furthermore, the SFI variation among individual rats in the negative control was very small and indicated that the lesion degree of the surgically-induced sciatic nerve injuries was similar and reproducible.

The ability to store water is one of the most important aspects of ECM, which supports various cellular activities and functions [39]. In reference to this, we examined the swelling capacity of the blending scaffolds in water. In an inversely proportional trend, as SF content decreased within the scaffold blends there was an increase in weight due to water absorption (Table 3). The observed changes in swelling are probably due to CS, because SF is a fibrous protein with a β-sheet structure and does not significantly swell. Moreover, CS contains primary amines and hydroxyl groups that provide a hydrophilic quality.

Tissue engineered scaffolds require appropriate mechanical and biological properties to retain the original shape and to support the tissue regeneration. In our study, we demonstrated that the mechanical properties can be manipulated by adjusting the SF content in CS/SF scaffolds. By increasing the concentration of SF, the elastic modulus, tensile strength and elongation-at-break of the scaffold all decreased (Table 1). A decrease of the elastic modulus can greatly improve the flexibility of the blend scaffolds, but the tensile strength and elongation-at break of the blend scaffolds make them too brittle for medical implantation. In our experiment, 7CS/3SF scaffolds demonstrated a favorable plasticity compared with that of 5CS/5SF scaffolds. The 5CS/5SF scaffolds became fragile

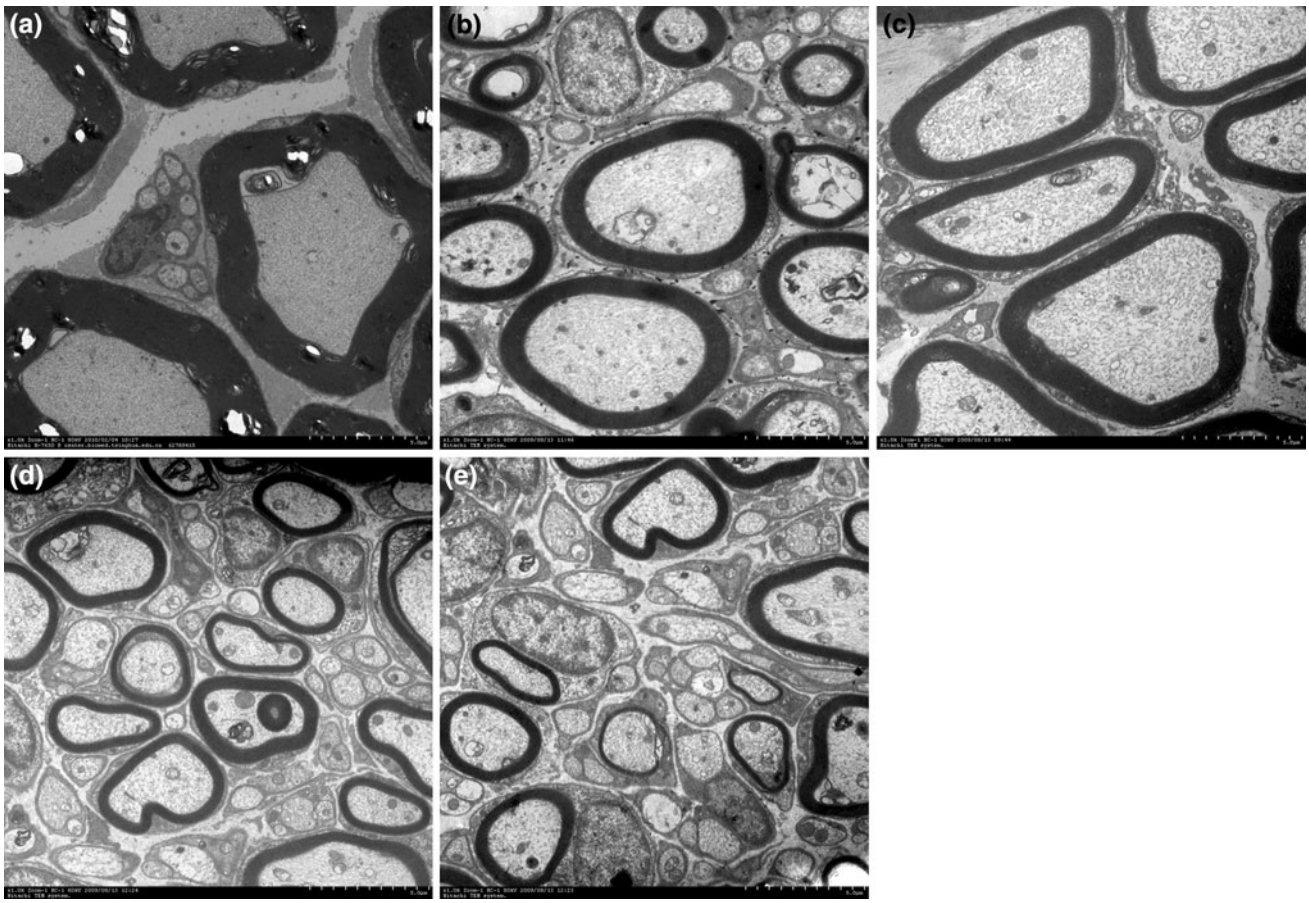

Fig. 13 Transmission election micrographs of middle sciatic nerve portion in positive control (**a**), SC-7CS/3SF scaffold group (**b**), ADSC-7CS/3SF scaffold group (**c**), 7CS/3SF scaffold group (**d**), and negative control group (**e**), respectively (*Scale bar* 5 μm)

Table 4 Comparison of stereological parameters of myelinated nerve fibers from the positive control and regenerated nerves

	Positive control	SC-7CS/3SF scaffold group	ADSC-7CS/3SF scaffold group	7CS/3SF scaffold group	Negative control group
Density of fibers (#/mm^2)	12488 ± 943	15983 ± 1024	18429 ± 3125	28800 ± 5286	26666 ± 5329
Fibers diameter (μm)	7.38 ± 0.68	6.38 ± 0.56	5.80 ± 0.45	4.65 ± 0.31	3.01 ± 0.37
Axons diameter (μm)	5.09 ± 0.14	4.67 ± 0.34	4.26 ± 0.23	3.58 ± 0.19	2.42 ± 0.46
Myelin thickness (μm)	1.17 ± 0.02	0.84 ± 0.05	0.75 ± 0.03	0.53 ± 0.07	0.36 ± 0.13
g-ratio	0.68 ± 0.01	0.73 ± 0.02	0.73 ± 0.04	0.76 ± 0.03	0.83 ± 0.03

Values means ± SD

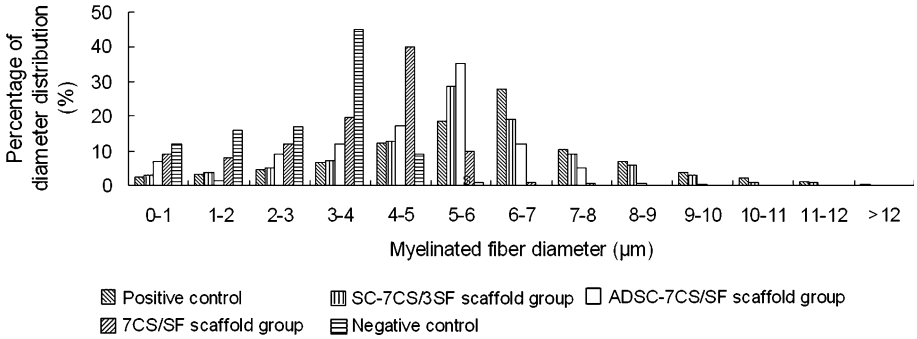

Fig. 14 Diameter distribution of myelinated nerve fibers at the middle sciatic nerve portion of the rat operated side

during fabrication. The tensile testing of the scaffold was performed by mimicking the surgical procedure to determine whether the scaffolds were too fragile for implantation. The suture retention strengths of pure CS alone and 7CS/3SF scaffold were high enough to resist the applied extension force, while the 5CS/5SF conduit was mechanically weak. The results were consistent with our observation and their mechanical properties. From in vitro experiments, the blend films efficiently supported adhesion and proliferation of SCs and ADSCs compared with that of CS alone (Figs. 3, 4). This observation may be due to the blended film surfaces containing amino acids from the SF component, which probably resulted in surface characteristics that enhanced cytocompatibility of CS/SF films.

To determine whether isolated cells from adipose tissue were rat ADSCs, passage 3–5 cells were analyzed by flow cytometry. Rat ADSCs were CD44 and CD90 positive, and CD11b, CD31 and CD45 negative, which is consistent with previous studies [36]. ADSCs express CD90 and lack hematopoietic lineage markers CD11b and CD45. In our previous study, isolated ADSCs were treated with factors that are known to induce differentiation toward adipogenic and osteogenic lineages. Von Kossa and oil red-O staining revealed that these ADSCs could differentiate into osteoblasts and adipocytes, which indicated multipotency similar to that of mesenchymal stem cells.

To evaluate grafted cell survival, cell viability and proliferation were determined by CCK-8. CCK-8 is non-radioactive and allows sensitive analysis of viable cells. The detection sensitivity of CCK-8 is higher than that of other tetrazolium salts such as MTT, XTT, MTS or WST [40]. Results showed that both SCs and ADSCs efficiently proliferated on 7CS/3SF scaffold, with 1.86-fold increase in SCs number and 2.14-fold increase in ADSCs number on day 7. Results indicated that SCs and ADSCs not only survived but also owned nice proliferation after grafted on the 7CS/3SF scaffold.

Considering the favorable physical and biological properties of CS and SF as mentioned above, we have developed a two-component artificial nerve scaffold seeded with ADSCs. In this novel design, the CS/SF scaffold supported nerve fiber re-growth, performed as a substrate for ADSCs delivery and allowed the diffusion of nutrients and other molecules while preventing fibroblasts from entering the injury. In the present study, myelinated axon diameter in the ADSC-7CS/3SF scaffold group was similar to that of the SC-7CS/3SF scaffold group, but much higher compared with those of the 7CS/3SF scaffold and negative control groups. Moreover, myelin sheath thickness at the repair site was the highest in the ADSC-7CS/3SF scaffold group compared with those in the 7CS/3SF scaffold and negative control groups. This could be because the functioning of the 7CS/3SF scaffold is only dependent on the single 7CS/3SF blending material without SCs or ADSCs. Following nerve injury and repair, fibroblasts invade the lesion site and contribute to scaring, which can impede axonal re-growth through the lesion and consequently impair functional recovery. One possibility for the improvement in regeneration following ADSCs transplantation is that the cultured ADSCs are "primed" to secrete trophic factors soon after transplantation, which rapidly provides trophic support for the injured axons. Without cell transplantation it takes endogenous SCs several days to detach from axons and up-regulate tropic factor expression [29]. Early ADSCs transplantation at the time of repair may allow rapid neurotrophic factor secretion that may prevent or reduce axonal dieback. In addition, transplanted ADSCs may rapidly integrate into the lesion site thereby limiting fibroblasts invasion that could impede axonal regeneration. Thus, ADSCs may provide trophic support that reduces axonal dieback and allows axonal regeneration to rapidly initiate and increase the probability of axon re-growth across the injury site. Furthermore, ADSCs may contribute to improved functional outcomes by differentiating into SCs in vivo and remyelinating regenerated axons.

The effect of ADSC-seeded scaffold grafts versus SC-seeded scaffolds, unseeded scaffolds and negative controls were investigated in a rat model of surgically-induced sciatic nerve injury with a 10 mm partial defect. Our fingdings suggest that enwrapping injured nerves with a CS/SF scaffold seeded with SCs and ADSCs, significantly improves axonal regeneration and locomotor recovery of injured hind limbs. These promising results from combining ADSCs with a CS/SF scaffold for nerve regeneration are positive steps toward future clinical applications in cases of peripheral nerve injury. Further studies are needed to determine the final phenotypic fate of engrafted cells in vivo and whether CS/SF-based tissue-engineered grafts seeded with ADSCs maintain beneficial effects in an entire nerve trunk transection model.

5 Conclusion

ADSC-seeded CS/SF scaffold implantation significantly improves axonal regeneration and functional recovery following surgically-induced sciatic nerve injuries. This effect may be due to two factors. One may be the sufficient mechanical strength of the scaffold, effective prevention of fibrous scar tissue invasion, and suitable permeation of nutrients and oxygen; the other may be the differentiation of ADSCs to SCs, relay and magnification of neurotrophic function from ADSCs to SCs in addition to ADSCs direct secretions of neurotrophic factors. This study provides evidence for the feasibility of ADSC-7CS/3SF scaffold use

in promoting nerve regeneration. Furthermore, our study establishes an experimental basis for clinical trial study to evaluate tissue engineered hybrid nerve grafts that are practical for implantation into peripheral nerves with partial sciatic nerve injuries.

Acknowledgments This work was supported by the National Natural Science Foundation of China (30670528, 30700848 and 30772443), National Basic Research Program of China (also known as the 973 Program, 2005CB623905) and the National Natural Science Foundation of Beijing (7082090).

References

1. Roglio I, Giatti S, Pesaresi M, Bianchi R, Cavaletti G, Lauria G, Garcia-Segura LM, Melcangi RC. Neuroactive steroids and peripheral neuropathy. Brain Res Rev. 2008;57:460–9.
2. Radtke C, Aizer AA, Agulian SK, Kankford KL, Vogt PM, Kocsis JD. Transplantation of olfactory ensheathing cells enhances peripheral nerve regeneration after microsurgical nerve repair. Brain Res. 2009;1254:10–7.
3. Ruch DS, Spinner RM, Koman LA, Challa VR, O'Farrell D, Levin LS. The histologic effect of barrier vein wrapping of peripheral nerves. J Reconstr Microsurg. 1996;12:291–5.
4. Dumanian GA, McClinton MA, Brushart TM. The effect of free fat grafts on the stiffness of the rat sciatic nerve and peripheral scar. J Hand Surg. 1999;24:30–6.
5. Amado S, Simões MJ, Armada da Silva PAS, Luís AL, Shirosaki Y, Lopes MA, Santos JD, Fregnan F, Gambarotta G, Raimondo S, Fornaro M, Veloso AP, Varejão ASP, Maurício AC, Geuna S. Use of hybrid chitosan membranes and N1E-115 cells for promoting nerve regeneration in an axonotmesis rat model. Biomaterials. 2008;29:4409–19.
6. di Summa PG, Kalbermatten DF, Pralong E, Raffoul W, Kingham PJ, Terenghi G. Long-term in vivo regeneration of peripheral nerves through bioengineered nerve grafts. Neuroscience. 2011;181:278–91.
7. Mohammadi R, Azizi S, Delirezh N, Hobbenaghi R, Amini K. Comparison of beneficial effects of undifferentiated cultured bone marrow stromal cells and omental adipose-derived nucleated cell fractions on sciatic nerve regeneration. Muscle Nerve. 2011;43(2):157–63.
8. di Summa PG, Kingham PJ, Raffoul W, Wiberg M, Terenghi G, Kalbermatten DF. Adipose-derived stem cells enhance peripheral nerve regeneration. J Plast Reconstr Aesthet Surg. 2010;63(9):1544–52.
9. Altman AM, Yan YS, Matthias N, Bai XW, Rios C, Mathur AB, Song YH, Alt EU. IFATS collection: human adipose-derived stem cells seeded on a silk fibroin-chitosan scaffold enhance wound repair in murine soft tissue injury model. Stem Cells. 2009;27:250–8.
10. Khor E, Lim LY. Implantation of chitin and chitosan. Biomaterials. 2003;24:2339–49.
11. Zheng ZH, Wei YJ, Wang G, Gong YD, Zhang XF. In vitro biocompatibility of three chitosan/polycation composite materials for nerve regeneration. Neural Regen Res. 2008;3:837–42.
12. Lv Q, Cao C, Zhang Y, Man X, Zhu H. The preparation of insoluble fibroin films induced by degummed fibroin or fibroin microspheres. J Mater Sci Mater Med. 2004;159:1193–7.
13. Yang YM, Chen XM, Ding F, Zhang PY, Liu J, Gu XS. Biocompatibility evaluation of silk fibroin with peripheral nerve tissues and cells in vitro. Biomaterials. 2007;28:1643–52.
14. Chalfoun CT, Wirth GA, Ewans GR. Tissue engineered nerve constructs: where do were stand? J Cell Mol Med. 2006;10:309–17.
15. Mirsky R, Jessen KR, Brennan A, Parkinson D, Dong Z, Meier C, Parmantier E, Lawson D. Schwann cells as regulators of nerve development. J Physiol Paris. 2002;96:17–24.
16. Rodriguez AM, Pisani D, Dechesne CA, Turc-Carel C, Kurzenne JY, Wdziekonski B, Villageois A, Bagnis C, Breittmayer JP, Groux H, Ailhaud G, Dani C. Transplantation of a multipotent cell population from human adipose tissue induces dystrophin expression in the immunocompetent mdx mouse. J Exp Med. 2005;201:1397–405.
17. Erba P, Terenghi G, Kingham PJ. Neural differentiation and therapeutic potential of adipose tissue derived stem cells. Curr Stem Cell Res. 2010;5:153–60.
18. Gardner RL. Stem cells and regenerative medicine: principles, prospects and problems. C R Biol. 2007;330:465–73.
19. Pittenger MF, Mackay AM, Beck SC, Jaiswal RK, Douglas R, Mosca JD, Moorman MA, Simonetti DW, Craig S, Marshak DR. Multilineage potential of adult human mesenchymal stem cells. Science. 1999;288:143–7.
20. Erickson GR, Gimble JM, Franklin DM, Rice HE, Awad H, Guilak F. Chondrogenic potential of adipose tissue-derived stromal cells in vitro and in vivo. Biochem Biophys Res Commun. 2006;290:763–9.
21. Lee JH, Kemp DM. Human adipose-derived stem cells display myogenic potential and perturbed function in hypoxic conditions. Biochem Biophys Res Commun. 2006;341:882–8.
22. Mehlhorn AT, Zwingmann J, Finkenzeller G, Niemeyer P, Dauner M, Stark B, Sudkamp NP, Schmal H. Chondrogenesis of adipose-derived adult stem cells in a poly-lactide-co-glycolide scaffold. Tissue Eng Part A. 2009;15:1159–67.
23. Zhu M, Kohan E, Bradley J, Hedrick M, Benhaim P, Zuk P. The effect of age on osteogenic, adipogenic and proliferative potential of female adipose-derived stem cells. J Tissue Eng Regen Med. 2009;3:290–301.
24. Zhu Y, Liu T, Song K, Ning R, Ma X, Cui Z. ADSCs differentiated into cardiomyocytes in cardiac microenvironment. Mol Cell Biochem. 2009;324:117–29.
25. Wang B, Han J, Gao Y, Xiao ZF, Chen B, Wang X, Zhao WX, Dai JW. The differentiation of rat adipose-derived stem cells into OEC-like cells on collagen scaffolds by co-culturing with OECs. Neurosci Lett. 2007;421:191–6.
26. Franco Lambert AP, Fraga Zandonai A, Bonatto D, Cantarelli Machado D, Pegas Henriques JA. Differentiation of human adipose-derived adult stem cells into neuronal tissue: does it work? Differentiation. 2009;77:221–8.
27. Caddick J, Kingham PJ, Gardiner NJ, Wiberg M, Terenghi G. Phenotypic and functional characteristics of mesenchymal stem cells differentiated along a Schwann cell lineage. Glia. 2006;54:840–9.
28. Wei YJ, Gong K, Zheng ZH, Liu LL, Wang AJ, Zhang LH, Ao Q, Gong YD, Zhang XF. Schwann-like cells differentiation of rat adipose-derived stem cells by indirect co-culture with Schwann cells in vitro. Cell Prolif. 2010;43(6):606–16.
29. Santiago LY, Clayiio-Alyarez J, Brayfield C, Rubin JP, Marra KG. Delivery of adipose-derived precursor cells for peripheral nerve repair. Cell Transpl. 2009;18:145–8.
30. Wei YJ, Zhou JL, Zheng ZH, Wang AJ, Ao Q, Gong YD, Zhang XF. An improved method for isolating Schwann cells from postnatal rat sciatic nerves. Cell Tissue Res. 2009;337:361–9.
31. Xu YF, Liu L, Li Y, Zhou C, Xiong F, Liu ZS, Gu R, Hou XM, Zhang C. Myelin-forming ability of Schwann cell-like cells induced from rat adipose-derived stem cells in vitro. Brain Res. 2008;1239:49–55.

32. She ZD, Zhang BF, Jin CR, Feng QL, Xu YX. Preparation and in vitro degradation of porous three-dimensional silk fibroin/chitosan scaffold. Polym Degrad Stab. 2008;93:1316–22.
33. Ao Q, Wang AJ, Cao WL, Zhang L, Kong LJ, He Q, Gong YD, Zhang XF. Manufacture of multimicrotuble chitosan nerve conduits with novel molds and characterization in vitro. J Biomed Mater Res A. 2006;77:11–8.
34. Wang AJ, Ao Q, Cao WL, Yu MZ, He Q, Kong LJ, Zhang L, Gong YD, Zhang XF. Porous chitosan tubular scaffolds with knitted outer wall and controlled inner structure for nerve tissue engineering. J Biomed Mater Res. 2006;79A(1):36–46.
35. Luís AL, Amado S, Geuna S, Rodrigues JM, Simões MJ, Santos JD, Fregnan F, Raimondo S, Veloso AP, Ferreira AJ, Armada-da-Silva PA, Varejão AS, Maurício AC. Long-term functional and morphological assessment of a standardized rat sciatic nerve crush injury with a non-serrated clamp. J Neurosci Methods. 2007;163:92–104.
36. Schäffler A, Büchle C. Adipose tissue-derived stromal cells-basic and clinical implications for novel cell-based therapies. Stem Cells. 2007;25:818–27.
37. Robinson LR. Traumatic injury to peripheral nerves. Muscle Nerve. 2000;23:863–73.
38. Stanec S, Tonkovic I, Stanec Z, Tonkovic D, Dzepina I. Treatment of upper limb nerve war injuries associated with vascular trauma. Injury. 1997;28:463–8.
39. Seddon H. Three types of nerve injury. Brain. 1943;66:237–88.
40. Munetaka I, Yoko M, Masanobu S, et al. Water-soluble tetrazolium salt compounds. US Patent no. 6063587; 2000.